High-power femtosecond optical pulse compression by using spatial solitons

D. H. Reitze, A. M. Weiner, and D. E. Leaird

Bellcore, 331 Newman Springs Road, Red Bank, New Jersey 07701

Received May 1, 1991

We demonstrate a novel pulse-compression technique that uses the self-confinement of two-dimensional spatial solitons propagating in bulk nonlinear media to increase the spectral bandwidth followed by a grating pair for recompression. Output pulses of 19-fs duration with 0.6-μJ energies are routinely obtained at a repetition rate of 8.6 kHz. Unlike other high-energy compression methods, soliton compression offers both high repetition rates and a potentially unlimited wavelength range.

Femtosecond pulse compression techniques that employ self-phase modulation in an optical fiber to generate spectral bandwidth have developed to the point where it is now possible to generate optical pulses as short as 6 fs.[1] However, fiber damage thresholds and parasitic higher-order nonlinear processes typically limit the amount of energy that can effectively be compressed to less than 10 nJ. Applications such as mode-selective excitation of coherent phonons by means of impulsive stimulated Raman scattering[2] and strong-field physics[3-5] require new methods of compression that produce short-duration optical pulses while maintaining high energies. In recent years progress has been made in extending the energy range of compressed pulses. Efforts by Rolland and Corkum, who used self-phase modulation in bulk materials, have succeeded in generating 100-μJ, 24-fs pulses.[6] Although this technique is applicable over a wide wavelength range, energies of at least 300 μJ are required, necessitating the use of a high-energy, low-repetition-rate amplifier system. Schoenlein *et al.*[7] and Boyer *et al.*[8] have produced 22- and 16-fs pulses, respectively, with ~0.5-μJ energies by amplifying and compressing broad-bandwidth pulses produced through continuum generation[7] or fiber coupling.[8] These techniques can be employed at kilohertz repetition rates; however, the choice of dyes available for broad-bandwidth amplification limits their wavelength range.

In this Letter we report on a new method of pulse compression, which produces 19-fs, 0.6-μJ optical pulses at a repetition rate of 8.6 kHz. Our method relies on the self-trapping and stable propagation of two-dimensional bright spatial optical solitons in bulk nonlinear media. In close analogy with temporal solitons, in which the balancing of group-velocity dispersion and self-phase modulation lead to dispersion-free propagation,[9] the balancing of diffraction by the spatial nonlinear index profile results in diffraction-free propagation.[10] Although self-trapping of beams in three dimensions is unstable and leads to catastrophic self-focusing, recent experiments have demonstrated the stable propagation of two-dimensional spatial solitons in CS_2 liquid[11] and in guided-wave geometries.[12-14] The self-trapped propagation of the spatial soliton itself maintains the high intensity necessary for large phase modulation, which generates the necessary bandwidth for pulse compression. Unlike other high-energy compression methods, soliton compression offers both high repetition rates and a potentially unlimited wavelength range.

The basic experimental apparatus for generating and compressing spatial solitons is as follows. Pulses of 75-fs duration and 0.1-nJ energies from a balanced colliding-pulse mode-locked ring dye laser operating at 620 nm were amplified to 30 μJ at a repetition rate of 8.6 kHz in a two-stage optical amplifier pumped by a 20-W copper-vapor laser. To achieve these pulse energies, we used a dye cell in the second stage.[15] Following recompression to 75 fs with a two-prism sequence in a double-pass geometry, the pulses were spatially filtered to improve beam quality and ensure the formation of clean spatial solitons. The energy throughput of the prism sequence–spatial filter was 11 μJ. We chose an 8-mm-thick piece of bulk fused silica as the nonlinear medium, which has a positive nonlinear index ($n_2 = 2.7 \times 10^{-16}$ cm^2/W), as required for bright spatial solitons as well as minimal linear and two-photon absorption. Pulses were focused on the front face of the glass in an elliptical profile by a cylindrical–spherical lens combination. We used beam diameters of $w = 900$ μm ($1/e$ peak intensity) in the long dimension (which we denote $\hat{x}$; see the graph of Fig. 1) and $a_{in} = 30$ μm in the short dimension (denoted $\hat{y}$). At low powers, the beam diffracts significantly only along the $\hat{y}$ dimension. At sufficiently high powers, nonlinear self-focusing balances diffraction, resulting in stable, nondiffractive soliton propagation. In the absence of filamentation, the beam profile in the long, $\hat{x}$ dimension should remain constant in the glass, since the sample length is less than the theoretical self-focusing distance. In order to ensure that filamentation did not occur, we used a two-beam interference technique.[11] A second beam, identical to the first, copropagates

0146-9592/91/181409-03$5.00/0

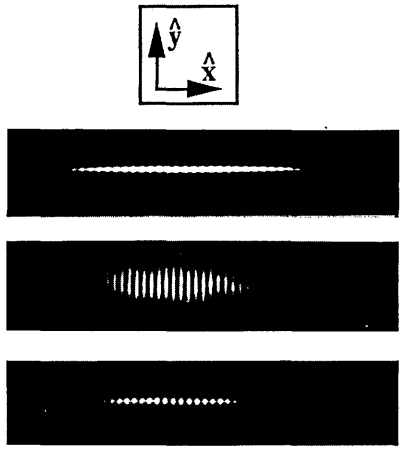

Fig. 1. Time-averaged spatial beam profiles at (a) the input face, (b) the output face (peak power 470 kW), and (c) the output face (peak power 47 MW). The fringes result from the interference of two beams, which prevents filamentation in the glass (explained in the text). Graph: $\hat{y}$ (soliton) and $\hat{x}$ (nonsoliton) dimensions.

simultaneously through the glass at a slight angle in the $\hat{x}$ dimension. The resulting interference fringes maintain the beams in narrow channels in which diffraction compensates for the self-focusing. Since the power contained in each channel is less than the critical power for self-focusing, each beam propagates without filamentation. To implement this procedure, the output from the spatial filter was split into two equal-energy beams in a conventional pump-and-probe geometry. The path length of each arm was adjusted for zero time delay at the front face of the glass. The angle between the two beams was set to 3° in the glass to minimize beam walk-off in the glass while maintaining a suitable interference fringe spacing (~30 μm) to ensure beam stability.

A small portion of the output was split off and used for diagnostic purposes. Soliton formation was monitored by imaging the output face of the glass onto a charge-coupled-device (CCD) camera. The output spectrum was monitored by imaging the elliptical output beams onto the entrance slit of a monochromator–optical multichannel analyzer (OMA). The slit was set parallel to $\hat{y}$ with a width of 50 μm (approximately 1/10 of the imaged beam) for spatial resolution of the spectral broadening. Only one of the two output beams was sent to the compressor. Following the fused silica, a second cylindrical–spherical telescope reshaped and collimated the beam. An adjustable slit placed parallel to $\hat{y}$ was then used to select the region of maximum spectral broadening. Pulses were compressed in a single pass through a pair of 600-line/mm gratings.[16] The transmission through the grating pair was 60%. Pulse durations were measured in a conventional noncollinear autocorrelator by using a 100-μm KDP crystal.

We first verified the formation and propagation of stable spatial solitons in the glass. Figure 1 presents beam profiles at both the input and output faces. At low powers [Fig. 1(b)] the beam has diffracted to 150 μm [five times the width at the front face shown in Fig. 1(a)], consistent with the expected diffraction given the 30-μm input width, the 8.0-mm path length, and $n_o = 1.46$ for fused silica. For a peak power of 47 MW [Fig. 1(c)] the beam has collapsed down nearly to the input width. At the soliton power $P_s = 2n_o w/n_2 a_o k^2$, nondiffractive propagation of the fundamental $N = 1$ soliton with beam diameter a_o will occur. Here k is the wave vector of the light in the glass. For our parameters, we expect propagation of an $N = 1$ soliton with $a_o = a_{in}$ at $P_s = 33$ MW. We note that, for powers that satisfy $0.25P_s < P < 2.25P_s$, stable, nondiffractive soliton propagation is expected but with a width a_o different from the input beam width a_{in}.[17] We therefore expect that some spectral broadening will occur even when $P < P_s$ because of the formation and propagation of solitons of width $a_{in} > a_o$. The beam shown in Fig. 1(c) is actually an integrated spatial profile, corresponding to a temporal average over the different spatial profiles resulting from different intensities contained within the temporal profile of the pulse. Unlike in previous experiments using ion-exchanged glass waveguides,[14,18] we saw no evidence of soliton deformation caused by two-photon absorption in our undoped, bulk fused-silica samples. This finding was corroborated by measuring the transmission through the glass as a function of input power. No measurable decrease in transmission was observed.

The spectra of the pulse before and after soliton formation are displayed in Fig. 2 for a peak power of 65 MW. In obtaining Fig. 2 we selected the high-intensity spatial region of the soliton in the $\hat{x}$ direction corresponding to the maximum spectral broadening. The observed width of 32 nm (5.3× broadening) is consistent with the expected

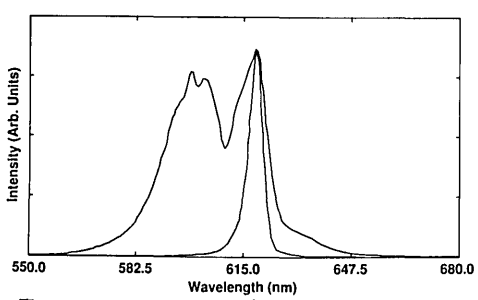

Fig. 2. Frequency spectra of pulses before ($\Delta\lambda = 6$ nm) and after ($\Delta\lambda = 32$ nm) soliton formation.

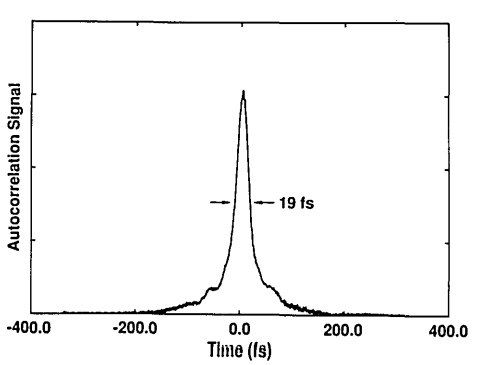

Fig. 3. Autocorrelation trace of a compressed pulse. The FWHM is 19 fs, assuming a sech^2 pulse shape.

broadening caused by self-phase modulation, given by[19] $\Delta\lambda_{out}/\Delta\lambda_{in} = [1 + (0.88\phi)^2]^{1/2} \approx 6$, where $\phi = 2\pi n_2 L I_{max}/\lambda_0$, $I_{max} = 3 \times 10^{11}$ W/cm^2 is the peak intensity in the glass, L is the path length, and λ_0 is the center wavelength. Lower-intensity regions of the beam showed decreased spectral broadening. It is important to note that appreciable spectral broadening was observed only when accompanied by soliton formation (as evidenced by a reduction in the output beam width), demonstrating that spatial soliton propagation is essential in achieving the spectral broadening necessary for compression. A representative autocorrelation trace of a compressed pulse is shown in Fig. 3. The FWHM of 19 fs (sech^2 pulse shape) gives a time–bandwidth product of 0.45, near the transform limit of 0.315. The slight energy present in the wings of the pulse could be completely suppressed by adjusting the grating separation at the expense of an increase in pulse width to 21 fs. Typical output pulse energies were 0.6 μJ. The spatial mode, measured by focusing the compressed, reshaped output with a 5× microscope objective and scanning the focal spot with a 2-μm pinhole, was Gaussian with a $1/e$ intensity diameter within 10% of the diffraction-limited value.

In addition to the expected variations in spectral broadening across the $\hat{x}$ beam profile, we also observed both an unexpected spatial variation (or chirp) in the center wavelength along $\hat{x}$ and nonsymmetric spectral broadening toward higher frequencies, as seen in Fig. 2. Moreover, measurements of the far-field output spatial profile revealed a deflection of the maximum intensity position with respect to the low power position. To understand these effects further, we repeated our experiments, using single beams. In the absence of the stabilizing beam, formation of the soliton at P_s was accompanied by filamentation in the nonsoliton ($\hat{x}$) dimension and continuum generation. We were able to avoid filamentation by working at $P = 0.8P_s$. The spectrum broadened to only 23 nm at the beam center; however, neither spatial chirp nor deflection was observed. The absence of spatial chirp in single-beam solitons suggests that two-beam stabilization is responsible for these unexpected effects. Pulses that are initially spatially overlapped will suffer both spatial and temporal walk-off as they propagate through the glass, owing to the finite propagation angle. In addition, each beam induces spatially and temporally varying refractive-index changes, which act as time-varying nonlinear prisms for the other. Finally, temporal broadening will occur as each beam propagates through the glass; consequently, the phase modulation induced on each beam by the other will be nonsymmetric in $\hat{x}$. A detailed analysis of these effects would examine the evolution of temporal, spatial, and spectral profiles during pulse propagation as influenced by diffraction, nonlinear refraction, group-velocity dispersion, self- and cross-phase modulation, and beam walk-off. Although such an analysis is beyond the scope of this Letter, we note that no spatial chirping effects were reported in previous picosecond spatial soliton experiments that used the two-beam stabilization technique.[11,12] This suggests that spatial chirping is due predominantly to femtosecond pulse durations, in which limited beam overlap and group-velocity dispersion play a significant role.

In summary, we have used the stable propagation of optical spatial solitons to compress optical pulses to durations of 19 fs while maintaining near-microjoule energies at 8.6-kHz repetition rates. Spatial soliton pulse compression combines both the wide wavelength range and high-energy throughput available from bulk nonlinear materials with the high repetition rates of copper-vapor laser-based amplifier systems. Finally, we note that this experiment is the first to our knowledge to examine the interplay of spatial and temporal optical nonlinearities that occur simultaneously as solitons propagate in nonlinear media.

It is a pleasure to acknowledge stimulating discussions with Y. Silberberg.

References

1. R. L. Fork, C. H. Brito-Cruz, P. C. Becker, and C. V. Shank, Opt. Lett. **12,** 483 (1987).
2. A. M. Weiner, D. E. Leaird, G. P. Wiederrecht, and K. A. Nelson, J. Opt. Soc. Am. B **8,** 1264 (1990).
3. H. M. Milchberg, R. R. Freeman, S. C. Davey, and R. M. More, Phys. Rev. Lett. **61,** 2364 (1988).
4. R. R. Freeman, T. J. McIlrath, P. H. Bucksbaum, and M. Bashansky, Phys. Rev. Lett. **57,** 3156 (1986).
5. M. C. Downer, G. Focht, D. H. Reitze, W. M. Wood, and T. R. Zhang, in *Ultrafast Phenomena VI,* T. Yajima, K. Yoshihara, C. B. Harris, and S. Shionoya, eds. (Springer-Verlag, Berlin, 1988).
6. C. Rolland and P. B. Corkum, J. Opt. Soc. Am. B **5,** 641 (1988).
7. R. W. Schoenlein, J.-Y. Bigot, M. T. Portella, and C. V. Shank, in *Ultrafast Phenomena VII,* C. B. Harris, E. P. Ippen, G. A. Mourou, and A. H. Zewail, eds. (Springer-Verlag, Berlin, 1990).
8. G. Boyer, M. Franco, J. P. Chambaret, A. Migus, A. Antonetti, P. Georges, F. Salin, and A. Brun, Appl. Phys. Lett. **53,** 823 (1988).
9. A. Hasegawa and F. Tappert, Appl. Phys. Lett. **23,** 142,171 (1973).
10. R. Y. Chiao, E. Garmire, and C. H. Townes, Phys. Rev. Lett. **13,** 479 (1964); V. E. Zakharov and A. B. Shabat, Sov. Phys. JETP **34,** 62 (1972).
11. A. Barthelemy, S. Maneuf, and C. Froehly, Opt. Commun. **55,** 201 (1985).
12. S. Maneuf, R. Desailly, and C. Froehly, Opt. Commun. **65,** 193 (1988).
13. J. S. Aitchison, A. M. Weiner, Y. Silberberg, M. K. Oliver, J. L. Jackel, D. E. Leaird, E. M. Vogel, and P. W. E. Smith, Opt. Lett. **15,** 471 (1990).
14. J. S. Aitchison, Y. Silberberg, A. M. Weiner, D. E. Leaird, M. K. Oliver, J. L. Jackel, E. M. Vogel, and P. W. E. Smith, J. Opt. Soc. Am. B **8,** 1290 (1991).
15. D. Nickel, D. Kühlke, and D. von der Linde, Opt. Lett. **14,** 36 (1989).
16. E. B. Treacy, IEEE J. Quantum Electron. **QE-5,** 454 (1969).
17. J. Satsuma and N. Yajima, Prog. Theor. Phys. Suppl. **55,** 284 (1974).
18. Y. Silberberg, Opt. Lett. **15,** 1005 (1990).
19. S. C. Pinault and M. J. Potasek, J. Opt. Soc. Am. B **2,** 1318 (1985).